MYCOSYNTHESIS OF HEMATITE (A-FE_2O_3) NANOPARTICLES USING FUNGI AND THEIR PHYSICO-CHEMICAL PARAMETERS AND PHOTOCATALYTIC ACTIVITIES.

Hazem Elsayed Kaabo1· Mahmoud H. Sultan1. Saad El-Din Hassan1· Hesham M. Mahdy1· Ebrahim Saied1.

[1] Department of Botany and Microbiology, Faculty of Science, Al-Azhar University, Nasr City, Cairo, Egypt

Corresponding author: prof.mahmoud@Azhar.edu.eg

ABSTRACT

Green approach for the synthesis of nanoparticles has been reported as the effective technique due to its ecofriendly, safe and applicable at large scale. The present study reports the green approach for hematite nanoparticle synthesis using *Aspergillus sydowii* using $FeSO_4 \cdot 7H_2O$ as a precursor. The biosynthesis of hematite is usually accompanied with changing in the color from colorless to yellow color and monitor using UV Vis-spectrophotometer.

The utilization of *Aspergillus sydowii* biomass filtrate for the biogenesis of hematite nanoparticles is the goal of the current work. The structural and optical properties of the fungal produced nanoparticles were investigated utilizing transmission electron microscopy (TEM), Fourier transform infrared spectroscopy (FTIR), x ray diffraction (XRD) and dynamic light scattering (DLS). All of the investigated parameters and their interactions were found to have a significant effect on the crystallite size, according to the results. The average diameter size of the biosynthesized Fe_2O_3-NPs was ranged between 20 -56 nm. The size of the biosynthesized Fe_2O_3-NPs was 28.7 nm, and their crystalline nature was confirmed by XRD, according to characterization results. A surface plasmon resonance spectrum of ferrous nanoparticles were obtained at 370 nm. Under UV light, Ribazol black b, safranin and crystal violet dyes were photo catalytically degraded utilizing biosynthesized Fe_2O_3 nanoparticles (NPs). The highest decolorization percentage of Ribazol black b, safranin and Crystal violet was 92.1% ± 1.2%, 70.1±0.88% and 94.3% ± 0.93%, respectively after 90 and 180 min, for Ribazol black b, safranin and crystal violet of incubation at 50.0 mg/mL^{-1} of Fe_2O_3-NPs. Furthermore, Fe_2O_3-NPs were successfully used more than once for biodegradation and that was regarded as its efficacy. hematite nanoparticles were used to remove Cb, Co, Pb, Zn and Cd, with percentages of 99.7 ± 1.2%, 99.1% ± 1.3%, 97.1% ± 1.3%, and 93.8% ± 1.4%, respectively. Finally the biosynthesized hematite nanoparticles were used for heavy metal bioremediation, and photocatalytic activity.

Keywords: Nanoparticles; Hematite; photocatalytic; fungi; Biosynthesis; Heavy metal removal; Dyes

1 Introduction

Nanotechnology is the science that deals with matter at the scale of 1 billionth of a meter (i.e., 10 − 9 m = 1 nm), In general, the size of a nanoparticle spans the range between 1 and 100 nm and is also the study of manipulating matter at the atomic and molecular scale **(Petersen, 2017).**

Nano-materials (NMs) have been developed in variety of forms such as nanowires, nanotubes, films, particles, quantum dots and colloids **(Bhat et al., 2018, Yaseen and Yaseen, 2019).** Nanoparticles (NPs) and nanomaterials (NMs) are now widely used in a variety of applications, including medicine, solar energy, drug delivery, water treatment, and pollution detection. Nanoparticles had been synthesized by different conventional methods such as sol-gel, aerosol, template assisted, sonochemical, laser exposer, wet-chemical synthesis, thermal decomposition, plasma synthesis, and hydrothermal synthesis often required several processing steps, controlled pH, temperature, pressure, much expensive equipment, and toxic chemicals **(Alzahrani et al., 2015; Dzido et al., 2015).** Furthermore, such techniques also generate several by-products which are toxic to ecosystems. So, there is a need to develop a low-cost, ecofriendly method for production of nanoparticles **(Jain et al., 2013; Tarafdar et al., 2012).**

Therefore, microbial systems are now being increasingly explored as safer alternatives for production of nanoparticles **(Raliya and Tarafdar, 2012; Kaul et al., 2012).** Synthesis of nanoparticles using fungi has several advantages over prokaryotic mediated approach regarding reproducibility of Nano sized materials, and these also include ease to multiplication, grow and handling, of Nano biosynthesis through Nano factories **(Jain et al., 2013).** Biological production systems are of special interest due to their effectiveness and flexibility **(Nithya et al., 2011).** Certain bacteria, fungi and plants express peptides or have a modified cell wall which binds to metal ions or metal salt, and these are able to form stable complexes in the form of nanoparticles **(Yong et al., 2002).**

Recently, different organisms such as bacteria, fungi, algae, and plants have been mediated for synthesis of hematite-NPs; however, the reduction occurs by combinations of biomolecules such as proteins, flavonoids and polysaccharides which significantly were produced by fungi **(Dhuper et al., 2012; Jain et al., 2013)**. Many fungi have been explored for nanoparticles synthesis such as *Aspergillus fumigates* **(Nithya et al., 2011),** *Aspergillus niger* **(Yong et al., 2002),** *Aspergillus oryzae* TFR9 **(Raliya, 2013)** and *Alternaria alternata* **(Sarkar et al., 2017).**

This study has aimed to biosynthesis of hematite-NPs using the biomass filtrate of fungus *Aspergillus* sp. as a capping agent. Identification of the fungal isolate well done by conventional technique in addition to molecular confirmation. Optimized physico-chemical parameter that influenced biosynthesis of hematite-NPs. Additionally, using nanoparticles for bioremediation and photocatalytic activities.

2 Materials and methods

All the chemicals, reagents, Czapex-yeast Autolyzate agar media (CYA), Czapex- Dox broth media (CDB), potato dextrose broth media (PDB), potato dextrose agar media (PDA), and sodium silicate were acquired from Sigma Aldrich and had a purity level of 99%. The precursor utilized was iron sulfate. In order to confirm the substance's photocatalytic characteristics, photo degradation operations on a few dyes were conducted. In this investigation, distilled water was used to complete every biological synthesis.

2.1 Isolation of fungal strain mediated synthesis of NPs

In the present study, water samples from harsh polluted old saltern were collected. Fungal isolate under study was isolated and purified. Water sample was collected from koom El Nawam, Damnhour, Al-Behera Governorate, Egypt (GPS N: 31°.40' 32", E: 30°.27' 48.81") in the winter of 2020s. 1 ml was inoculated on potato dextrose agar (PDA) plates supplemented with chloramphenicol to suppress bacterial growth **(Qayyum et al., 2016).** Triplicates of plates were used. Then, the plates were incubated for seven days at 28°C until colonies detected. The purified colonies were sub-cultured and preserved for further work on PDA slantes.

2.2 Identification of fungal strains

The fungus was isolated and identified on specific culture medium used for fungi, Czapek Yeast Agar (CYA). Identification of fungal isolate was carried out according to the following references: Raper and Fennell (1965), Booth and Kenkel (1986), Domsch et al., (1980), and Moubasher and moustafa (1970).

Phenotypic identification was confirmed by partial genotypic sequencing of Internal Transcribed Spacer (ITS1) region was amplified between the ribosomal genes (rDNA) 18S - 5.8S using universal primers: 5.8S - 28S ITS1 (5'-TCCGTAGGTGAACCTGCGG-3'), (White, 1990, White *et al*., 1990).

3 Nanoparticle synthesis

3.1 Biosynthesis of hematite nanoparticles.

Two disk of freshly purified fungal specie was inoculated in 100ml Czapex Dox Broth (CDB) medium (Sucrose 30g, NaNO3: 2g, KH 2HPO4:1g, KCl: 0.5g, MgSO4.7H2O: 0.5g, FeSO4.7H2O: 0.01g and Distilled water: 1000ml) and incubated at 28±2^{o}C for 5 days in rotary orbital shaker 150 rpm. At the end of incubation period, fungal biomass was harvested by passing through four layer of medical gauze. The harvested fungal biomass for each fungal species was washed with sterilized distilled water to remove any medium components. Then, ten g of fungal biomass was suspended in 100 ml distilled water for 72h at 28±2^{o}C. After incubation period, biomass filtrate was obtained by passing it through sterile whatman filter paper No.1. The obtaining biomass filtrate was collected and used for biosynthesis of hematite-NPs as the following: 1.0 mM FeSO4.7H2O was added to 100 ml of biomass filtrate for 24 h

(Raliya, 2013). After that, most potent fungal isolate used for biosynthesis of hematie-NPs was selected according to color change and maximum absorbance resonance peaks which detected using UV-Vis spectrophotometer **(JENWAY 6305 Spectrophotometer).**

3.2 Factors affecting nanoparticle synthesis

Using UV–Vis spectroscopy, a Jenway 6305 Spectrophotometer, (Jenway, Staffordshire, UK) was used to measure the maximum surface plasmon resonance, which allowed the investigation of the parameters influencing the synthesis and dispersion of NPs. These included pH values (3.0–10.0), time of contact between biomass filtrate and NPs precursors (12, 24, 36, 48 and 72 h), precursor (iron sulfate) concentrations (1.0–5.0 mM), and incubation temperature of the biomass filtrate and metal ions (25, 30, 35, and 40 °C). Incubation periods for fungal biomass in distilled water were also taken into consideration. On a nanoparticle that had its SPR value previously discovered, these variables were measured. The highest absorbance peaks at 280 nm for Fe_2O_3-NPs were measured to determine the ideal circumstances.

3.3 Instrumental analysis of the optimized Fe_2O_3-NPs.

The subsequent characterization techniques were used to ascertain the physical characteristics of the obtained post-biotransformation Fe_2O_3-NPs under ideal circumstances. The form and size of the biosynthesized Fe_2O_3-NPs were investigated using transmission electron microscope analysis **(TEM) (JEOL 1010, Japan).** The samples were made by drop- coating the Fe_2O_3-NPs solution onto a copper grid that had been coated with carbon. The color shift caused by the production of NPs was observed using UV–Vis spectroscopy (**JENWAY 6305 Spectrophotometer)** at a wavelength of 200–800 nm. The crystallinity of biosynthesized Fe_2O_3-NPs was further examined using XRD patterns on a Philips X'Pert Pro X-ray diffractometer **(Eindhoven, Netherlands).** The range of the 20 was between 4-$^{\circ}$ and 80°C. The X-ray source was Cu-Ka radiation that had been Ni-filtered. There was a 40 kV voltage and a 30 mA cur-rent. The Debye Scherrer equation was used to determine the average size of NPs produced from the fungal metabolites **(Hassan et al., 2021)**. Using DLS analysis, it was possible to determine the sizes and distribution of biosynthesized metal oxide NPs in colloidal solutions. The samples were reconstituted in distilled water before being measured by DLS using a Nano ZS Zeta **Sizer (Malvern, UK).** Through the measurement of the polydispersity index (PDI), DLS analysis can reveal information regarding the homogeneity of NP solutions **(Ateeb M et al., 2023)**. Finally, using Fourier transform infrared (FTIR) Spectroscopy **(Agilent System Cary 660 FTIR model),** it was determined how fungal metabolites and various functional groups contributed to the reduction, capping, and stabilization of Fe_2O_3-NPs. To produce FTIR spectra, the materials were scanned between 400 and 4000 cm-$^{-1}$ **(Hashem and Salem, 2022)**.

4 Catalytic activities against crystal violet, safranin and Ribazol black b dyes

In the presence of UV light, the ability of bio-fabricated Fe_2O-NPs to break down crystal violet, safranin and Ribazol black b as a dye model was studied. Each Fe_2O_3-NPs concentration (30 and 50 mg L-$^{-1}$) was independently added to the crystal

violet, safranin and Ribazol black b solution (50 mg L^{-1}) for a variety of contact periods (30, 60, 90, 120, and 150 min). The CV and Ribazol black b solutions were stirred at room temperature for 25 min prior to the experiment to achieve the equilibrium of absorption and desorption between the dye solutions and the surface of the Nano catalyst **(Muhiuddin et al., 2023)**. The effectiveness of each Fe_2O_3-NPs concentration to adsorb or degrade the crystal violet, safranin and Ribazol black b solutions was evaluated in comparison to the control (crystal violet, safranin and Ribazol black b solutions without Fe_2O_3-NPs separately) by mixing the Nano catalyst and the crystal violet, safranin and Ribazol black b solutions under light settings with air bubble aeration. 2 mL of each treatment were taken out at regular intervals and centrifuged for 15 min at 3000 rpm. A crystal-clear supernatant was collected. The M-ETCAL spectrophotometer was then used to measure their optical density at a maximum λ max of crystal violet, safranin and Ribazol black b solutions at 664 nm. The following equation was used to compute the percentages of color removal:

$$Decolorization percentages(\%) = D - D1/D \times 100 \quad (1)$$

Where D is the initial absorbance and D1 is the final absorbance at interval times.

The trapping approach was used to look into the role that various reactive species, including hydroxyl radicals (•OH), superoxide radicals ($\bullet O_2^-$), and holes (h^+), play in the break-down of crystal violet, safranin and Ribazol black b. In this procedure, reaction solutions containing 20 g/mL^{-1} of green produced Fe_2O_3-NPs to 10 mg/L^{-1} of crystal violet, safranin and Ribazol black b solution were added separately for 150 min under UV light irradiation at pH 7 the reaction solutions containing 1 mM of isopropyl alcohol (IPA), 1 mM of benzoquinone (QB), and 1 mM of ethylene diaminetetraacetate (EDTA). These substances, in turn, serve as quenchers for •OH, O_2^-, and h^+. Following the contact period, the mixture's absorbance was determined to be 664 nm, and the degradation percentages were then deter-mined as previously described. To boost the dye adsorption even further, the catalyst's reusability was examined over the course of six cycles. The nano-catalyst was used in the second cycle after being retrieved from the first cycle and having undergone three washes with distilled water to eliminate any leftover water.

5 The in vitro heavy metals adsorption by Fe_2O_3-NPs

Using a PerkinElmer Analyst 800 atomic spectrometer, the key common heavy metals in wastewater, including Hg, Co, Pb, Cd, and Ni, were evaluated both before and after NPs treatment. Atomic absorption spectroscopy relies on the free metallic ions' ability to absorb light to detect heavy metals. To test the silica nanoparticles ability to adsorb the selected metals, aquarium water was introduced with a metal con-centration of 100 ppm. To assess the adsorption capacity of Fe_2O_3-NPs, water samples were obtained after 24 h **(Malik LA et al., 2019)**. Atomic Absorption Spectrophotometer was carried out in the Faculty of Veterinary Medicine, Zagazig University, Egypt.

6 Statistical analysis

Data collected in the present study are presented as the means of three independent replicates and subjected to statistical analysis using the statistical package

SPSS v17. The mean difference comparison between the treatments was analyzed by t-test or the analysis of variance **(Tsivileva et al., 2021)**, and it was subsequently analyzed by the Tukey HSD test at $p < 0.05$.

7 Results and discussion

7.1 Potency of the fungal isolate NW5 for Fe_2O_3-NPs biosynthesis

Out of 18 fungal isolates obtained, the isolate NW5 appeared to biosynthesize Fe_2O_3-NPs. This isolate was identified at the genus level morphologically as *Aspergillus* sp.

7.2 Isolation and identification of fungal isolate

Among the fungal isolates from extreme environments under study NW5 was selected upon

its activity to biosynthesize Fe_2O_3-NPs.

7.2.1 Macroscopic characteristics of *Aspergillus* sp.

Colony diameters on CYA reached 30-33 mm in 10 days at 28°C, plane to slightly floccose texture; with deep grayish blue surface, while ivory red or maroon reverse was found.

7.2.2 Microscopic characteristics

Conidial heads are radiate, spherical to loosely columnar with light gnaphalium green shades. Hyaline conidiophores ends with spherical (or nearly so) vesicles bearing two series of conidiogenous cells; biseriate, having phialides that arise from sterile metulae. The conidia are roughly spherical, and measure 2.5–4.5 μm in diameter.

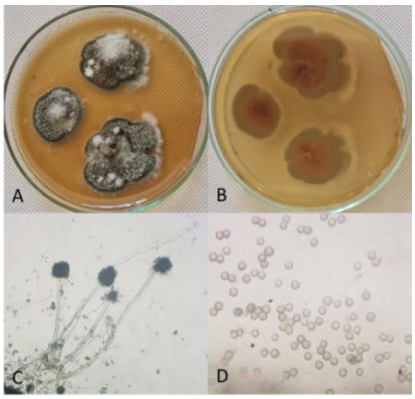

Fig (1):

A. Colony observe of ***Aspergillus* sp.** on CYA grown at 28°C for 10 days showing the culture characteristics

B. Colony reverse of ***Aspergillus* sp.** on CYA grown at 28°C for 10 days showing reverse pigmentation
C. Light microscope showing stipe and conidial head of ***Aspergillus* sp.** (Mag. power 200X).
D. Light microscope showing rough walled conidia of ***Aspergillus* sp.** (Mag. power 800X).

7.2.3 Molecular identification.

The sequence of the amplified ITS1 fragment (525 bp) showed 100 % homology with other sequences of related *Aspergillus sydowii* strains recorded in Gene Bank, and then it was set down at the NCBI database with accession number PP309809 as *Aspergillus sydowii* strain Sultan, MH - NW5.

A phylogenetic tree based on the ITS1 region sequences with other reference *Aspergillus* species recorded in NCBI Gene Bank was created to investigate the phylogenetic relations of the strain under study. The results showed that *Aspergillus sydowii* PP309809 belongs to the *Aspergillus sydowii* species with a bootstrap value of more than 99% and in the same clade.

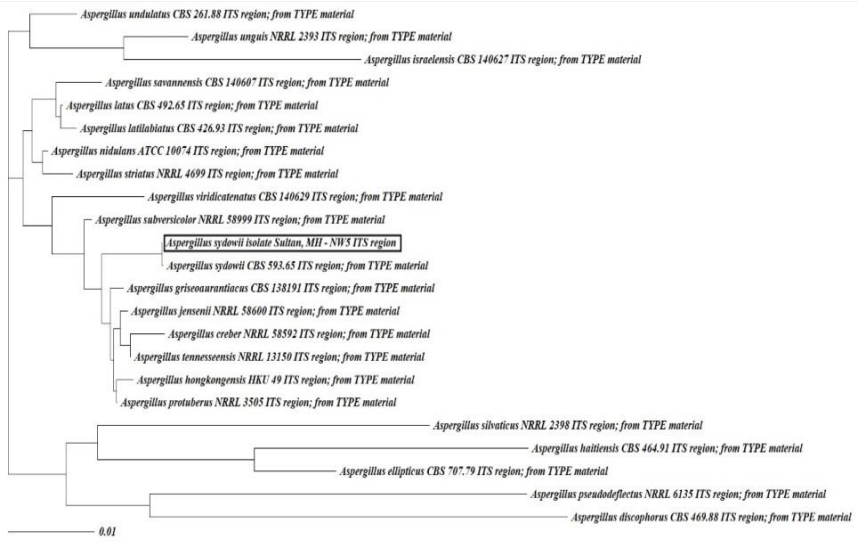

Fig (2) Bootstrap maximum-likelihood phylogenetic trees of *Aspergillus sydowii* strain PP309809 based on ITS1 region sequences, the graph shows clustering with *Aspergillus* spp.

7.3 Green synthesis of hematite nanoparticles (Fe_2O_3-NPs).

Aspergillus spp. have the ability to synthesize various NPs and the fungal based NP biosynthesis, intracellular and extracellular enzymes and biomolecules reduce various metal ions as part of the bio mineralization process **(Annamalai et al., 2021)**. Through the process of intracellular synthesis, metal salt is added to the fungal culture, causing the biomass to produce and internalize nanoparticles. To disrupt the fungal biomass and extract the nanostructures, a variety of techniques are used, including

centrifugation, filtration, and chemical treatment. In order to produce non-aggregating nanoparticles in the medium, the more popular extracellular approach entails combining the metal precursor with the fungal filtrate that contains the biomolecules **(Yamini and Rajeswari, 2022)**.

In this study, *Aspergillus sydowii* strain PP309809 was isolated from salt water sample and study their ability to biosynthesis of hematite-NPs through extracellular mechanism to select most potent isolates. Extracellular mechanism depends on the reduction of iron salt by nitrate reductase enzyme. While, the other secreted proteins in biomass filtrate stabilize the performed hematite -NPs **(Fouda et al., 2017).** The reduction of $FeSO_4.7H_2O$ is commonly accompanied with color change of biomass filtrate from colorless to reddish brown after adding $FeSO_4.7H_2O$. Also biosynthesis of hematite -NPs was accompanied with absorption spectra to detect maximum surface Plasmon resonance. Therefore, biomass filtrate for *Aspergillus sydowii* strain PP309809 showed high intensity for reddish brown color compared to control (Fig.3). Also showed the maximum surface plasmon resonance at wavelength 370nm (Fig.4) **(Mahdavi et al., 2013)**. Hence, *Aspergillus sydowii* strain PP309809 was selected as most potent for further study.

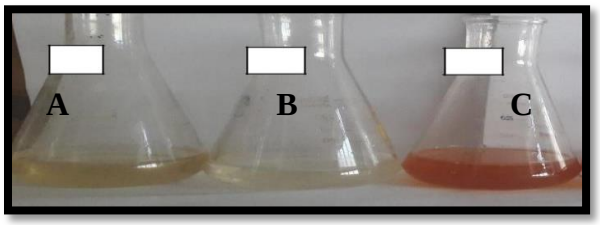

Fig (3): Color change of hematite-NPs synthesized using *Aspergillus sydowii* strain PP309809:A) $FeSO_4.7H_2O$ without biomass filtrate. B) Biomass filtrate and C) Color change for *Aspergillus sydowii*

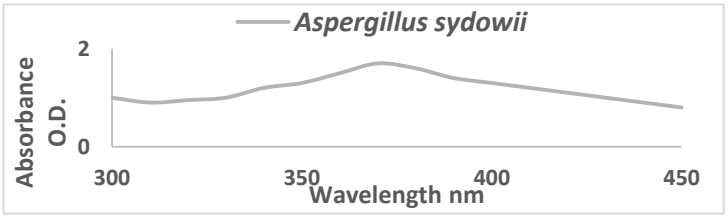

Fig (4): UV spectrum of reaction mixture of 1 mM $FeSO_4.7H_2O$ with biomass filtrate of *Aspergillus sydowii* showed maximum Plasmon resonance at 370 nm.

7.4 Optimization of the physiochemical parameters for Fe_2O_3-NPs biosynthesis

7.4.A Factors affecting on fungal growth.

Factors affecting on the growth of *Aspergillus sydowii* were achieved according to the following technique. The biomass filtrate obtained from the fungal biomass grown under different condition is subjected to $FeSO_4.7H_2O$ and then

allowed to produce hematite-NPs. At the end of each factor, the absorbance of the formed hematite-NPs is measured using UV-Vis Spectra at wavelength 370 nm.

7.4.A.1 Effect of different incubation periods.

Data represented in Table 1 showed the effect of different incubation periods on growth of *Aspergillus sydowii* and on the biosynthesis of hematite-NPs. According to our data the absorbance at 370 nm was increased with increasing the incubation period up to 7 days. This, clearly, refers to biosynthesis of hematite-NPs was affected by incubation period which lead to increasing the reduction potency of the biomass filtrate. Nevertheless, by increasing the incubation period over 7 days, the absorbance decreased according to aggregation of nanoparticles. **(Sastry, 2003),** is followed to study iron nanoparticles formation by *Pleurotus* sp. The culture was kept under shaking conditions (200rpm) for 96h. On the other hand, **(Ahmad et al., 2006)** reported that, the biomass of *Penicillium* sp. and *Aspergillus niger* were harvested after 3 days. And **(Al-Askar et al., 2013)** reported that, the best incubation period for harvested of biomass of *Fusarium oxysporum* was achieved after 7 days.

7.4. A. 2 Effect of incubation temperatures.

Incubation temperature plays a critical role not only on fungal growth but also on nanoparticles productivity. The data represented in Table 1 indicate that, the absorbance at 370nm was increased by increasing the incubation temperatures up to 32°C. This, clearly, refers to increase the formation of hematite-NPs with incubation temperatures due to enzyme and Protein was stable at specific temperature. Nevertheless, by increasing the incubation temperature over 32°C, the absorbance decreased according to aggregation of nanoparticles. Similar results have been recorded by **(Bellı et al., 2004). (Subha Rajam et al., 2013)** and (**Vala et al., 2012)** found that, the *Aspergillus* sp. and *Aspergillus niger* were inoculated in liquid media at room temperature.

7.4. A.3 Effect of different pH values on hematite-NPs production.

The data represented on Table 1 showed the effect of different pH values on growth of *Aspergillus sydowii* strain PP309809 for biosynthesis of hematite-NPs, and the absorbance at 370nm increases up to 6 pH values. This, clearly, refers to enzyme and protein responsible for reduction potency was stable at pH 6 while instable at lower or above pH value. These results agree with previous work obtained by (**Immanuel et al., 2007)** and **(Fouda et al., 2017)**, found that the fungus culture *Aspergillus* sp. was grown aerobically in CDB medium at 6 pH. Other reports found that the fungus culture *Aspergillus terreus* was grown in broth medium at a pH of 6.8 **(Azeem et al., 2018**). The optimum pH value for almost fungal growth in acidic medium, so that the high yield of metabolic activity of *Aspergillus sydowii* strain PP309809 increasing at pH 6. Below and above this optimal pH value, the metabolic activity decrease gradually.

8.4. A.4 Effect of different inoculum sizes (Disks).

The data represented in Table 1 indicate that, the absorbance at 370nm was increased with increasing the inoculum sizes up to 3 disks (7mm) of fungal culture. This, clearly, refers to increase the formation of hematite-NPs with inoculum sizes due to increasing biomass growth which lead to high reduction potency. Nevertheless, by increasing the inoculum sizes over 2 disks, the absorbance decreased. Similar data represented by (**Fouda et al., 2017)** which found that, inoculation of 50 ml of broth media with two disk was the optimum inoculum for biosynthesis of nanoparticles.

Table (1): Optimization factors affecting on growing of Aspergillus sydowii and biosynthesis of hematite nanoparticles.

Different incubation periods								
Days	**3**	**4**	**5**	**6**	**7**	**8**	**9**	**10**
O.D. at 370nm	0.70± 0.01	0.79± 0.033	0.82± 0.017	0.98± 0.052	1.21± 0.015	1.13± 0.015	1.11± 0.016	1.17± 0.038
Incubation temperature(°C)								
Temp. (°C)	**25 °C**	**28 °C**	**32 °C**	**35 °C**	**40 °C**			
O.D. at 370nm	0.34±0.009	0.73±0.012	1.13±0.019	0.79±0.041	0.71±0.015			
Initial pH values								
pH	**5**	**6**	**7**	**8**	**9**	**10**		
O.D. at 370nm	0.91±0.0134	1.12±0.015	0.82±0.0173	0.88±0.086	0.69±0.023	0.64±0.009		
Inoculum size (Disks)								
No. of disk	**1** disk	**2** disk	**3** disk	**4** disk				
O.D. at 370nm	0.70±0.018	0.92±0.028	1.20±0.125	1.18±0.015				
Biomass with distilled water (Days)								
Days	**1**	**2**	**3**	**4**				
OD. at 370nm	0.89±0.012	0.91±0.020	1.15±0.013	1.12±0.008				

7.4. A.5 Effect of incubation periods between biomass and distilled water.

The incubation periods of biomass with distilled water play an important role in section of enzyme and protein responsible for reduction potency of biomass

filtrate. The data from Table 1 showed, the biosynthesis of hematite-NPs refereed by absorbance was increased gradually to attain their maximum value after 3 days. Which lead to increase the amount of fungal secreted enzymes and proteins which increasing the formation of hematite-NPs, after three days, the absorbance decreased. In the same manner, **(Mazumdar and Haloi, 2017)** and (**Bhainsa and D'souza, 2006)** succeeded to prepare iron nanoparticles and AgNPs after 72h duration period. While, others suspended biomass of *Aspergillus niger* with sterile double distilled water for preparing Ag-NPs obtained at 48 hrs. **(Ninganagouda et al., 2014).**

Mean± SEr of *Aspergillus* sydowii at absorbance 370nm.

7.4. B. Factors between biomass filtrate of *Aspergillus sydowii* and $FeSO_4.7H_2O$.

Factors controlling the productivity of hematite-NPs were achieved according to the following technique. The biomass filtrates of *Aspergillus sydowii* is subjected to $FeSO_4.7H_2O$ and then allowed to produce hematite-NPs under different physico-chemical parameters. The absorbance of the performed hematite-NPs was measured using UV-Vis Spectra at wavelength 370 nm.

7.4.B.1 Effect of different pH value between biomass filtrate and $FeSO_4.7H_2O$.

Table 2 showed the effect of pH value between biomass filtrate of *Aspergillus sydowii* and precursor of hematite-NPs which adjusted using buffer solution for adjusting pH from 6 to11 according to **(Lundblad and Macdonald, 2010).** Results showed that, increasing the absorbance of the formed hematite-NPs was recorded at pH value (10). Increasing the pH over than 10, the absorbance of hematite-NPs is significantly decreased. This behavior could be attributed to the stabilizing proteins secreted by fungi, in turns, preventing the formed hematite-NPs from aggregation. The secreted proteins become more stable and attractive to iron salt in moderate alkali medium. Similar result at pH10 for production of AgNPs recorded by **(Rabie et al., 2015).** Other studies found that, the maximum production of AgNPs was obtained at alkaline pH 8.2 **(Velu et al., 2017).** Another report showed that the production of iron oxide nanoparticles by *Bacillus subtilis* at pH9 **(Sundaram et al., 2012).**

7.4.B.2 Effect of different temperatures between biomass filtrate and $FeSO_4.7H_2O$.

Data represented in Table 2 revealed that the absorbance increase with increasing temperatures from 25°C to 45°C. highly productivity of hematite nanoparticles were obtained at 35°C by *Aspergillus* sydowii. **(Latha and Gowri., 2014)** reported the use of an extract of Carica papaya leaves as an effective reductant for making Fe_3O_4-NPs (33 nm, spherical) at normal room temperature. Other reported found that, Silver nanoparticles were synthesized at incubation temperature between biomass filtrate and precursor was 25°C **(Shafiq et al., 2016).** While FeCl3

and the extracts of different parts of plants were used to produce Fe-NPs at 50–60^{o}C **(Shah et al., 2014).**

7.4.B.3 Effect of different concentration of $FeSO_4.7H_2O$ on the biosynthesis of hematite-NPs

Data reported in Table 2 Showed the UV-visible spectra of hematite-NPs which affected by concentration of $FeSO_4.7H_2O$. Maximum productivity for hematite-NPs were obtained at 3.0 mM of $FeSO_4.7H_2O$. On the other hand, **(Raliya et al., 2014a) and (Kumar et al., 2008),** reported that, the cell free filtrate of *Aspergillus oryzae* TFR9 was treated with 1mM FeCl3.6H2O and *Aspergillus foetidus* were treated with 1mM AgNO3 to obtaining maximum productivity respectively. **(Sarkar et al., 2017)** reported that, the concentration of FeCl3.6H2O used for synthesis

7.4.B.4 Effect of incubation time between biomass filtrate and $FeSO_4.7H_2O$.

As shown in Table 2, the optimal incubation time to produce maximum extracellular hematite-NPs when biomass filtrate of *Aspergillus* sydowii treated with 3mM $FeSO_4.7H_2O$ solution was 24h. Other reported found that, the maximum yield of iron nanoparticles was achieved at 12 hours. When cell filtrate of *Aspergillus oryzae* TFR9 was treated with 1mM of salt solution of FeCl3 **(Raliya et al., 2014b).** Other report found that, the highest formation for iron oxide nanoparticles by bacillus subtilis is around 80 h of incubation **(Sundaram et al., 2012).**

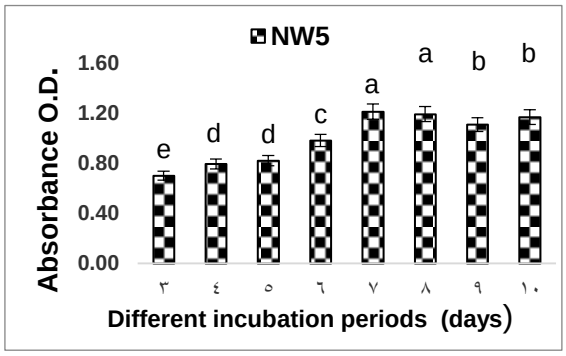

Fig. 5. Effect of different incubation periods on hematite-NPs production (Days). Where, NW5, *Aspergillus sydowii*.

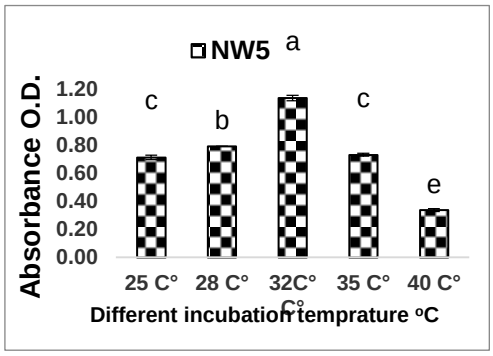

Fig. 6. Effect of different incubation temperatures on hematite-NPs production. Where, NW5, *Aspergillus sydowii*.

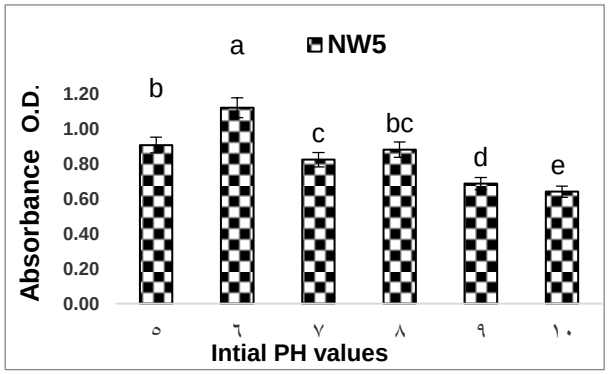

Fig. 7. Effect of different pH values on hematite-NPs production. Where NW5, *Aspergillus sydowii*.

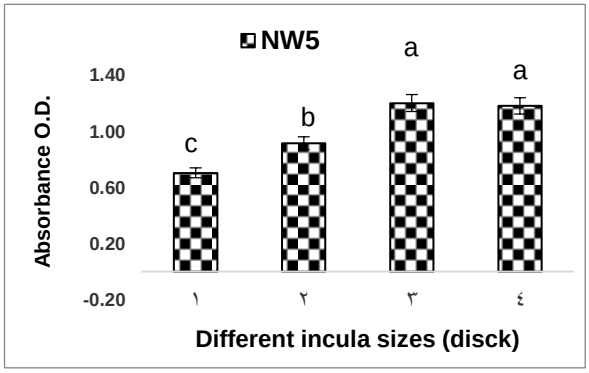

Fig. 8. Effect of different inoculum sizes on hematite-NPs production (Disks). Where, NW5, *Aspergillus sydowii*.

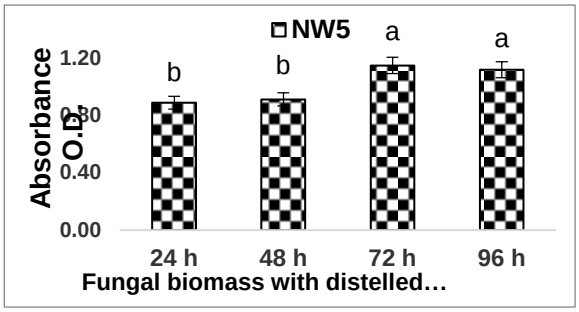

Fig. 9. Effect of incubation periods of the reaction between fungal biomass and distilled water. Where, NW5, *Aspergillus sydowii*.

Table (2): Factors affecting on the reaction between biomass filtrate and $FeSO_4.7H_2O$.

Table (2): Optimization factors affecting on growing of *Aspergillus sydowii* and biosynthesis of iron oxide nanoparticles.						
Different pH values						
pH	**5**	**6**	**7**	**8**	**9**	**10**
OD. at 370nm	0.64±0.015	0.69±0.017	0.82±0.013	1.12±0.025	1.32±0.015	1.63±0.012
Incubation temperature(°C)						
Temp. (°C)	**25 °C**	**30 °C**	**35 °C**	**40 °C**		
O.D. at 370nm	1.11±0.015	1.43±0.018	1.63±0.018	1.56±0.008		
Different FeSO4.7H2O concentrations						
FeSO4.7H2O Concentrations	**1 mM**	**2 mM**	**3 mM**	**4 mM**	**5 mM**	
O.D. at 370nm	0.70±0.0136	0.92±0.022	0.82±0.017	0.88±0.086	1.66±0.027	
Different incubation time (h.)						
Incubation Time (h.)	**12 h**	**24 h**	**36 h**	**48 h**	**72 h**	
O.D. at 370nm	0.82±0.017	0.92±0.028	1.32±0.018	1.18±0.015	1.08 ±0.013	

Mean± SEr of *Asperagillus* sydowii at absorbance 370nm.

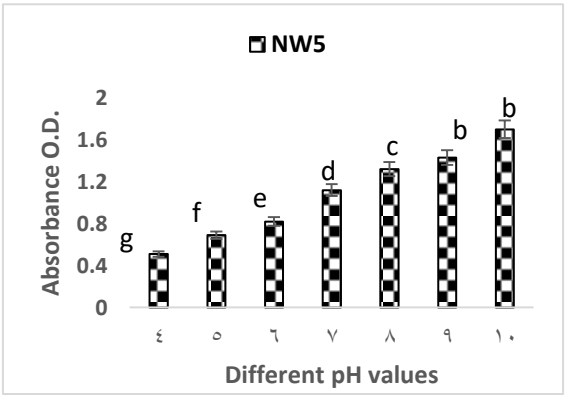

Fig. 10. Effect of different pH values on the reaction between biomass filtrate and FeSO4.7H2O.

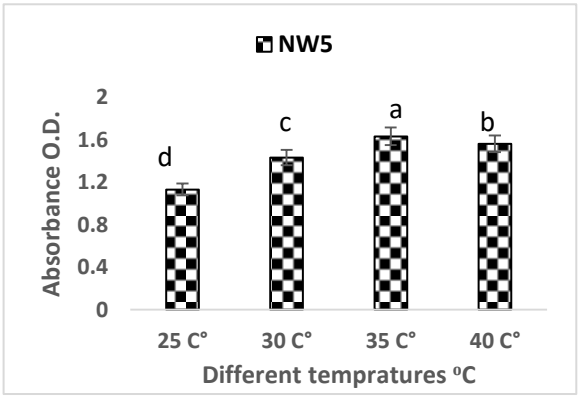

Fig. 11. Effect of different temperatures on the reaction between biomass filtrate and FeSO4.7H2O. Where. NW5. *Asperaillus svdowii*.

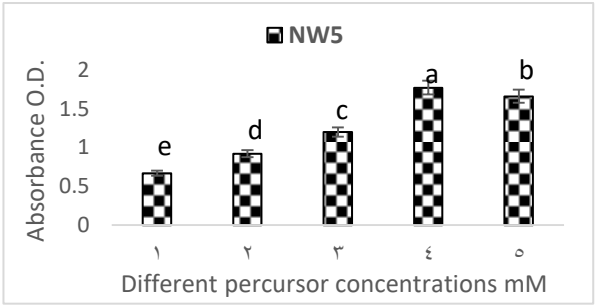

Fig. 12. Effect of different concentration of FeSO4.7H2O for biosynthesis of hematite-NPs by three fungal isolates.

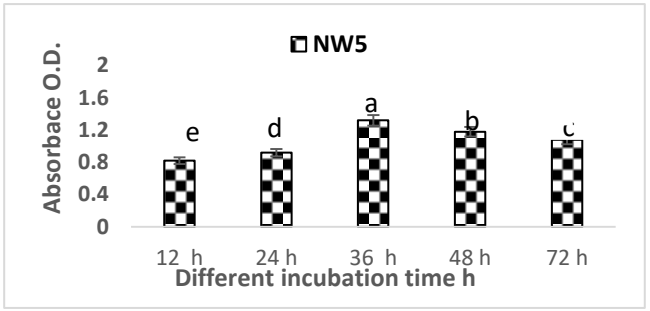

Fig. 13. Effect of different incubation times between biomass filtrate and FeSO4.7H2O. Where, NW5, *Aspergillus sydowii*.

8.5 Characterization of hematite nanoparticles produced by *Aspergillus sydowii*.

The creation of nanoparticles and their shape are guaranteed by the characterization of the generated product (i.e., Fe_2O_3-NPs). The general characteristics of nanoparticles are their size, shape, absorbance, and disparity. For the study of the nature and morphologies of nanoparticles, conventional characterization techniques, including spectroscopic and microscopic processes, are used. The size and form of a nanoparticle have a significant impact on its qualities. Advanced characterization procedures are necessary since nanoparticles are invisible to the naked eye. TEM examination was used to determine the size, shape, and morphology of the produced Fe_2O_3-NPs.

8.5.1 Transmission electron microscope (TEM).

TEM images revealed the size and shapes of hematite-NPs synthesized by *Aspergillus sydowii*. Fig (14) Showed spherical shape of hematite -NPs synthesized by *Aspergillus sydowii* with sizes range of 25-65 nm and 20-60 nm, respectively.

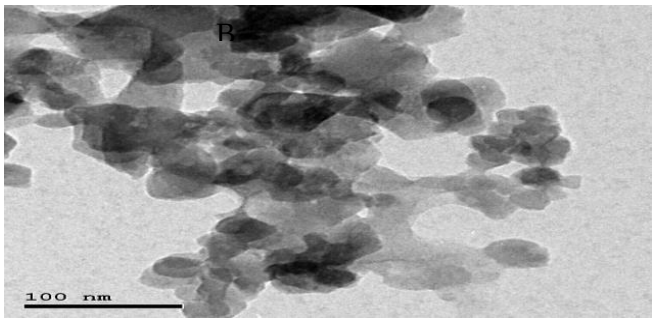

Fig. (14) TEM micrograph for biosynthesized Hematite-NPs. B, Hematite-NPs synthesized using *Aspergillus sydowii.*

8.5.2. Fourier transform infrared Spectroscopy (FTIR).

FTIR spectra for obtained purified powdered hematite nanoparticles were carried out to identify possible interaction between hematite and protein molecules, which may be responsible for biosynthesis, stabilization as well dispersed hematite nanoparticles in the reaction mixture. Data represented in (Fig. 5) Revealed intense absorption peaks appear at 3371.70, 1612.39, 1426.73, 1062.46, 995.87, 815.60, 663.09, 600.49 and 508.24 cm^{-1}, 3412.02, 3252.66, 1629.57, 1496.68, 1076.32, 1012.80, 816.66, 663.56, 621.39, 601.96, 516.98 and 411 cm−1 for hematite nanoparticles

synthesized by *Aspergillus sydowii* showed respectively. The peaks at 3412.02, 3371.70 and 3252.66cm^{-1} corresponds to O-H stretching group of phenols and alcohol and may be due to the N-H asymmetric stretch mode of amines. The bands at 1629.57, 1612.39 and 1496.68 cm^{-1} corresponded to the binding vibrations of amide I band of protein with N–H stretching. The bands observed at1076.32, 1062.46 and 1012.80 cm^{-1} may be assigned to C–N stretching vibrations of aromatic and aliphatic amines. The peaks at 516.98, 508.24 and 411 cm^{-1} were corresponded to alkene (=C-H bending). Free amino or carboxyl groups present in proteins that found in biomass filtrate which can bind with FeO-NPs.

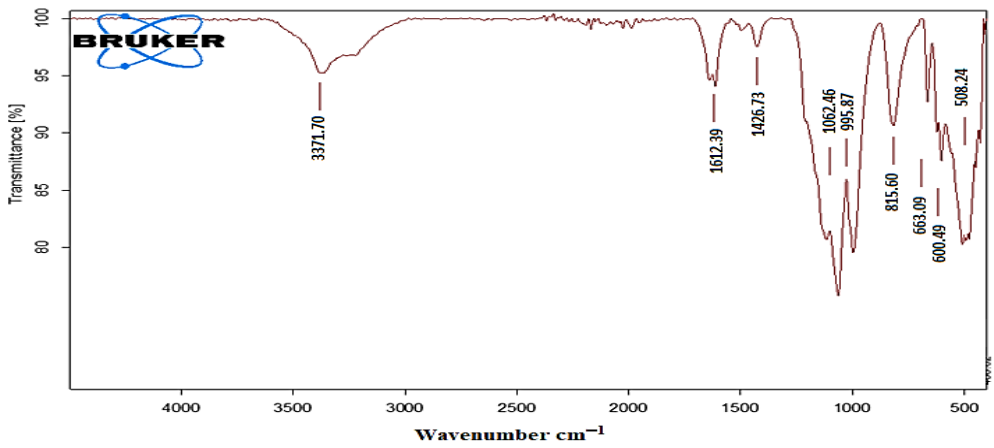

Fig. (15). FTIR spectra for hematite -NPs synthesized by *Aspergillus sydowii*.

8.5. 3. X-ray diffraction (XRD) analysis.

X-ray diffraction can be used to confirm the crystalline nature of the particles using JCPDS (JCPDS card no. 01-079-0007). XRD pattern has been obtained represented in (Fig. 6). The XRD intense peaks corresponding to (012), (104), (110), (113), (024), (116), (122), (214) and (300). That clearly confirm to hematite nanoparticle synthesis *by Aspergillus sydowii* and suggests that the Hematite-NPs were essentially in the face centered cubic structure and crystal in nature. The average size determined by Scheer equation for hematite nanoparticles synthesized by *Aspergillus sydowii* were 67.4 and 64.55, respectively.

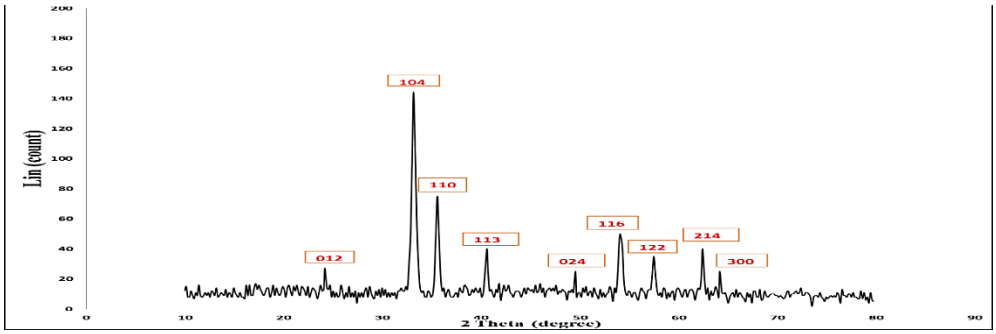

Fig (16). XRD pattern of hematite nanoparticles synthesized by *Aspergillus* sydowii.

8.5.4. Particle size and zeta analysis

According to the particle size analysis, it was found that the particle size determination of the biosynthesized hematite nanoparticles was based on intensity that represented in (Fig. 7). Laser diffraction revealed that, the particles obtained were poly-dispersed in mixture. The hematite nanoparticles synthesized by Aspergillus sydowii, showed the average diameter of the particles were found to be 79.7 and 85.8 nm, respectively. Poly-dispersity indexes (PDI) of the biosynthesized hematite-NPs using *Aspergillus sydowii*, was found to be 0.021 and 0.028 respectively which showed the biosynthesized nanoparticles are poly-dispersed. The Zeta potential graphs of hematite -NPs are given in (Figs. 8). The Zeta potential of green synthesized hematite -NPs was +25 mV and -35 mV for *Aspergillus sydowii*.

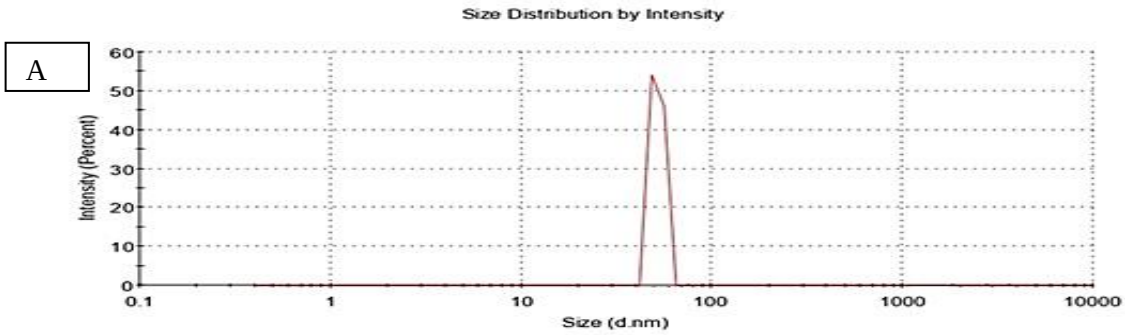

Fig. (17). DLS showing the size distribution profile of biosynthesized hematite-NPs using A, *Aspergillus sydowii.*

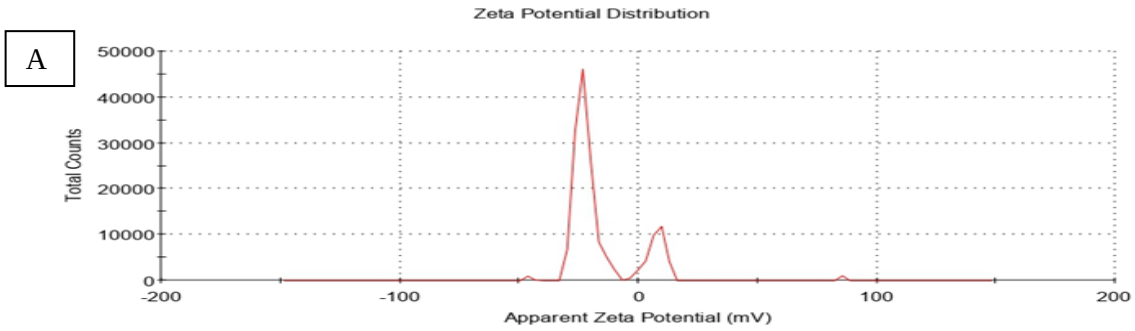

Fig. (18) Zeta potential showing the size distribution profile of biosynthesized hematite-NPs using A, *Aspergillus sydowii*

dyes by using Fe_2O_3-NPs.

The efficacy of the biosynthesized hematite-NPs for decolorization of dye effluents obtained from the different textile factories were investigated. In this experiment, the dye effluents were treated by biosynthesized hematite-NPs at different concentrations represented as 30 and 50 mg/100 ml at different time course. According to the high decolorization percentages, we select the best concentration of nanoparticles at specific time course.

8.6.1Treatment of three Dyes effluents (Ribazol black B, Crystal violet and Safranin) by 30 mg of biosynthesized hematite-NPs.

Data represented graphically in fig. (9.10.11) showed the capacity of 30 mg of hematite-NPs for decolonization of different dye effluents at different time courses. Data revealed that the decolorization percent was significantly increased with time. For dye Ribazol black B, the decolorization percent after 180 min was 52.1 % While the highest decolorization percentages of crystal violet dye after 180 min was 61.5 % and decolorization percentages for safranin dye after 180 min was 50.1 % for Hematite-NPs synthesized by *Aspergillus sydowii*

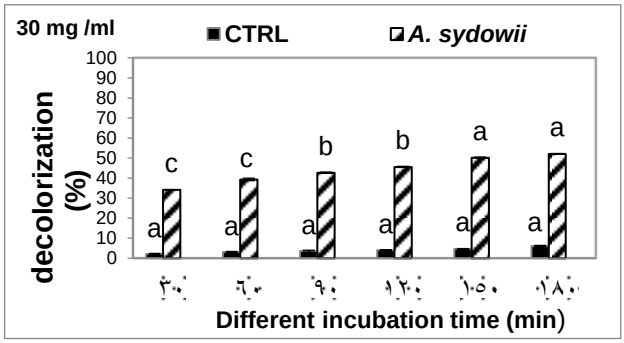

Fig. 19. Decoloization percent of Ribazol black B after treatment with 30 mg of hematite-NPs at different time courses.

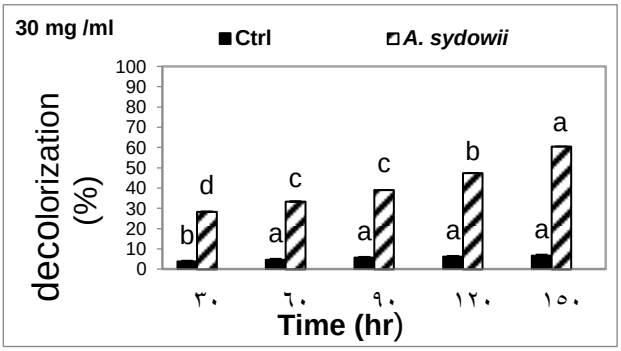

Fig. 20. Decoloization percent of crystal violet after treatment with 30 mg of hematite-NPs at different time courses.

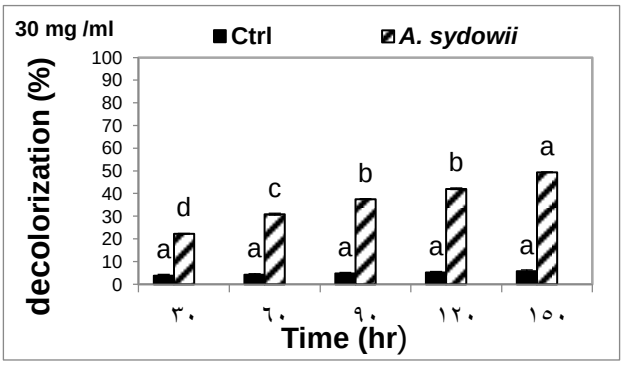

Fig. 21. Decoloization percent of safranin after treatment with 30 mg of hematite-NPs at different time courses.

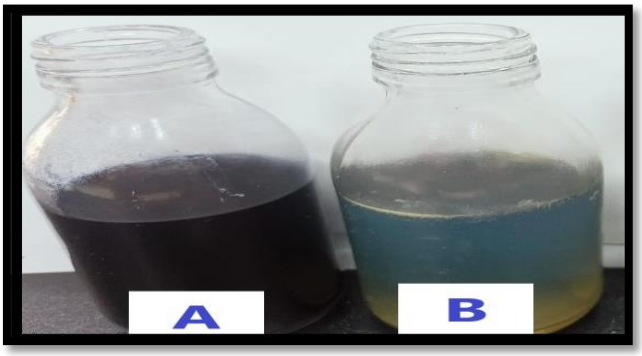

Photo. 22. Color change of Ribazol Black B due to treatment by 30 mg of hematite-NPs at different time course. Where, A) control; B) hematite-NPs synesthized by *A. sydowii*

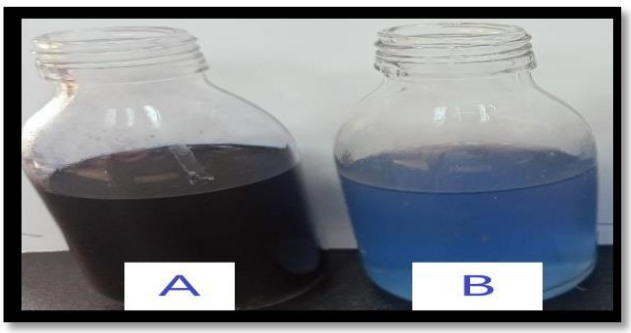

Photo. 23. Color change of Crystal violet due to treatment by 30 mg of hematite-NPs at different time course. Where, A) control; B) hematite-NPs synesthized by *A. sydowii*

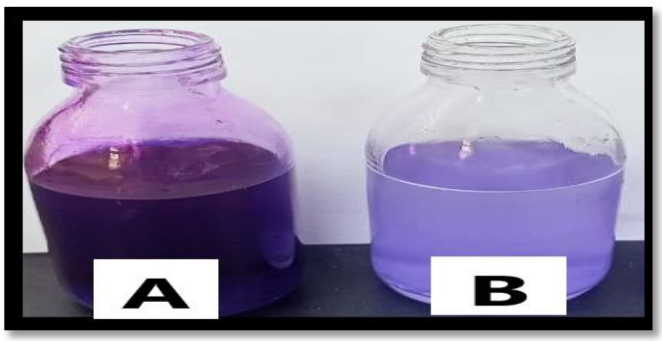

Photo. 24. Color change of Safranin due to treatment by 30 mg of hematite-NPs at different time course. Where, A) control; B) hematite-NPs synesthized by *A. sydowii*

8.6.2Treatment of three Dyes effluents (Ribazol black B, Crystal violet and Safranin) by 50 mg of biosynthesized hematite-NPs.

Data represented graphically in fig. (9.10.11) showed the capacity of 50 mg of hematite-NPs for decolonization of different dye effluents at different time courses. Data revealed that the decolorization percent was significantly increased with time. For dye Ribazol black B, the decolorization percent after 180 min was 92.1 % While the highest decolorization percentages of crystal violet dye after 180 min was 94.3 % and decolonization percentages for safranin dye after 180 min was 70.1 % for Hematite-NPs synthesized by *Aspergillus sydowii*.

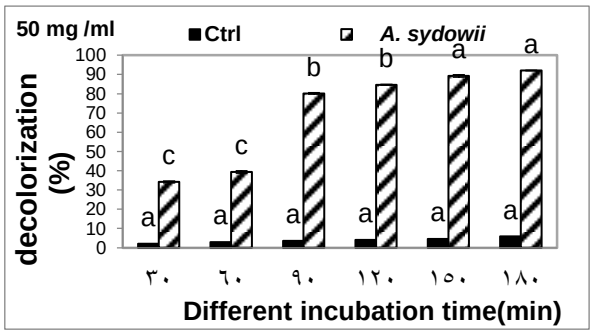

Fig. 25. Decolorization percent of Ribazol black B after treatment with 50 mg of hematite-NPs at different time courses.

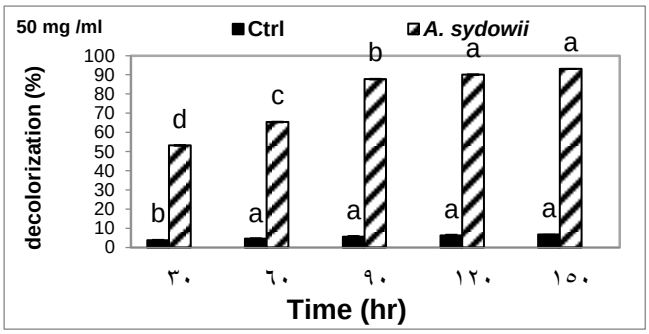

Fig. 26. Decolorization percent of crystal violet after treatment with 50 mg of hematite-NPs at different time courses.

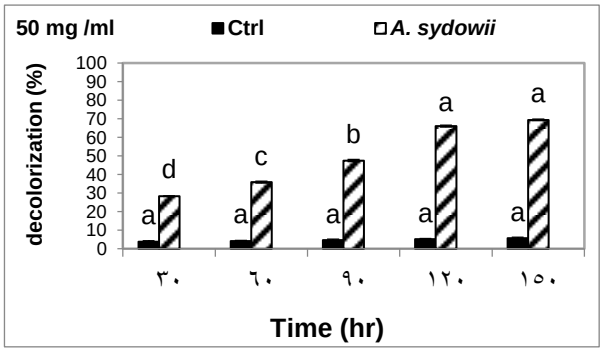

Fig. 27. Decolorization percent of safranin after treatment with 50 mg of hematite-NPs at different time courses.

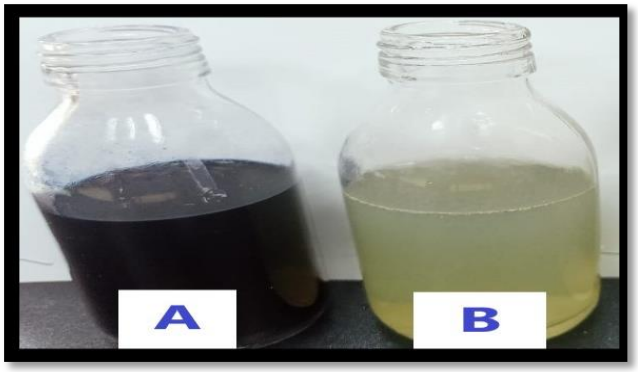

Photo. 28. Color change of Ribazol Black B due to treatment by 50 mg of hematite-NPs at different time course. Where, A) control; B) hematite-NPs synesthized by *A. sydowii*

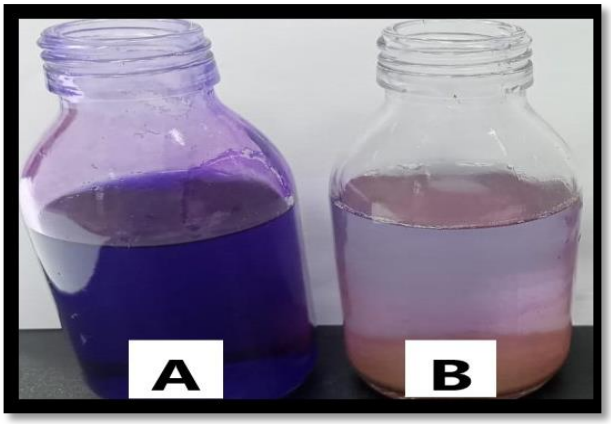

Photo. 29. Color change of Crystal violet due to treatment by 50 mg of hematite-NPs at different time course. Where, A) control; B) hematite-NPs synesthized by *A. sydowii*.

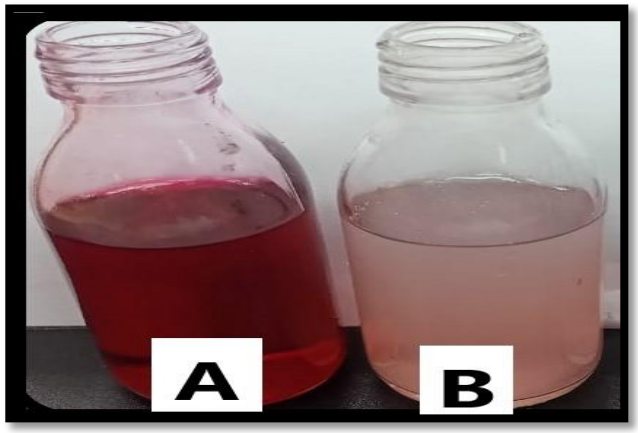

Photo. 30. Color change of Safranin due to treatment by 50 mg of hematite-NPs at different time course. Where, A) control; B) hematite-NPs synesthized by *A. sydowii*.

8.7 Removal of some heavy metals by NPs treatments.

From the data represented in table (3). The removal of heavy metals was decreased near to hundred percent for all heavy metals were measured. The adsorption efficacy showed that, increasing the removal percent of cobalt (99.9 %) due to treatment by hematite-NPs synthesized by *A. sydowii* as compared to control, for other metals the high adsorption percent was 97.5, 85.6 and 99.7 % for Cobalt, lead and cadmium due to hematite-NPs synthesized by *A. sydowii*.

Table 3. Heavy metals removal due to NPs treatments (50mg) of FeO-NPs for 24h

NPs	**NPs synthesized by *A. sydowii***	**Co**	**Zn**	**Pb**	**Cd**
Treatments		mg\L - ratio %	mg\L - ratio %	mg\L - ratio %	mg\L - ratio %
Control		13.817 0	31.3 0	24.521 0	34.668 0
After NPs treatment	*A. sydowii*	0.115 99.1%	0.717 97.7%	1.51 93.8%	0.072 99.7%

CO, Cobalt; Zn, Zinc; Pb, Lead and Cd, Cadmium.

9 Conclusion

The biosynthesis of nanoparticles by microorganisms is rapid, it provides satisfactory biosynthesis of nanoparticles and the whole process is very cheap and effective without the involvement of hazardous chemicals by a rapid and simple procedure. Iron oxide nanoparticles were successfully synthesized by *Aspergillus sydowii* strain PP309809 using extracellular protein. The various physico-chemical parameters such as concentration of precursor, pH of extract and incubation temperatures plays an important role in biosynthesis of iron oxide nanoparticles. The color change occurs due to surface plasmon resonance during the reaction for reduction of precursor used which confirmed by UV-Vis spectroscopy.

The microbial-mediated synthesis of Fe_2O_3-NPs exhibits a greater advantage over other conventional techniques as it produces a uniform, spherical shape NPs, respectively. The biogenic synthesis of Fe_2O_3-NPs was achieved through an extracellular method using a cell-free filtrate of *A. sydowii*, which led to the production of spherical nanoparticles with sizes range of 25-65 nm and 20-60 nm. FTIR measurement provided strong evidence for the presence of proteins and functional groups that stabilize and prevent the agglomeration of the particles. Synthesized nanoparticles were found to be capable of photocatalytic crystal violet, safranin and Ribazol black b dye degradation. Iron nanoparticles showed the maximum enhancement in photocatalytic activity of dyes 94.1% and 85.1%, respectively. The Fe_2O_3-NPs exhibited high adsorption capabilities for heavy metals, making them promising bioadsorbents for the eco- friendly removal of these pollutants, which remove Co, Pb, Cd, and Zn with percentages of 99.1%, 93.8%, 99.7%, and 97.7%, respectively.

REFERENCES

Ahmad, I.; Ansari, M.I. and Aqil, F. (2006)*:* Biosorption of Ni, Cr and Cd by metal tolerant *Aspergillus niger* and *Penicillium* sp. using single and multi-metal solution. Indian journal of experimental biology, 44, 73-76.

Al-Askar, A.A.; Hafez, E.E.; Kabeil, S.A. and Meghad, A. (2013): Bioproduction of silver-nano particles by *Fusarium oxysporum* and their antimicrobial activity against some plant pathogenic bacteria and fungi. Life Sci J, 10(3), 2470-2475.

Alzahrani, E.; Sharfalddin, A. and Alamodi, M. (2015); Microwave-hydrothermal synthesis of ferric oxide doped with cobalt. Advances in Nanoparticles, 4(02), p.53.

Annamalai, J., Ummalyma, S. B., Pandey, A., & Bhaskar, T. (2021). Recent trends in microbial nanoparticle synthesis and potential application in environmental technology: a comprehensive review. Environmental science and pollution research international, 28(36), 49362–49382.

Ateeb, M., Asif, H. M., Ali, T., Baig, M. M., Arif, M. U., Farooq, M. I., … Shaukat, I. (2023). Photocatalytic and Antibacterial activities of bio-synthesised silver nanoparticles (AgNPs) using Grewia asiatica leaves extract. *International Journal of Environmental Analytical Chemistry*, 1–19.

Azeem, M.; Saleem, Y.; Hussain, Z.; Zahoor, S. and Javed, M.M. (2018): Optimization of Culture Conditions for the Production of Lovastatin by Aspergillus Terreus in Submerged Fermentation. Pharmaceutical Chemistry Journal, 52(3): 284289.

Bellı, N.; Marın, S.; Sanchis, V. and Ramos, A.J. (2004): Influence of water activity and temperature on growth of isolates of Aspergillus section Nigri obtained fromgrapes. International journal of food microbiology, 96(1): 19-27.

Bhainsa, K.C. and D'souza, S.F. (2006): Extracellular biosynthesis of silver nanoparticles using the fungus *Aspergillus fumigatus*. Colloids and surfaces B: Biointerfaces, 47(2): 160-164.

Bhat, A. H., Rehman, W. U., Khan, I. U., Khan, I., Ahmad, S., Ayoub, M. and Usmani, M. A. (2018). Nanocomposite membrane for environmental remediation. In Polymer-based Nanocomposites for Energy and Environmental Applications (pp. 407-440).

Booth, T. & Kenkel, N. (1986). Ecological studies of lignicolous marine fungi: a distribution model based on ordination and classification. In Moss, S.T. (ed.): *The biology of marine fungi*. pp: 297-310.

huper, S.; Panda, D. and Nayak, P.L. (2012): Green synthesis and characterization of zero valent iron nanoparticles from the leaf extract of *Mangifera indica*. Nano Trends: J Nanotech App, 13(2): 16-22.

Domsch, K. H.; Gams, W. and Anderson, T. H. (1980). Compendium of Soil Fungi" *Academic Press, Inc. New York.*

Dzido, G.; Markowski, P.; Małachowska-Jutsz, A.; Prusik, K. and Jarzębski, A.B. (2015): Rapid continuous microwave-assisted synthesis of silver nanoparticles to achieve very high productivity and full yield: from mechanistic study to optimal fabrication strategy. Journal of Nanoparticle Research, 17(1): p. 27.

Fouda, A.; Saad, E.; Elgamal, M.S.; Mohmed, A.A. and Salem, (2017): Optimal factors for biosynthesis of silver nanoparticles by *Aspergillus* sp. In Al Azhar Bulletin of Science, Conf, March 2017; 9th. P. 161-172.

Hashem AH, Salem SSJBj (2022) Green and ecofriendly bio-synthesis of selenium nanoparticles using Urtica dioica (stinging nettle) leaf extract: Antimicrobial and anticancer activity. 17(2): 2100432.

Hassan, S. E., Fouda, A., Saied, E., Farag, M. M. S., Eid, A. M., Barghoth, M. G., Awad, M. A., Hamza, M. F., & Awad, M. F. (2021). Rhizopus oryzae-Mediated Green Synthesis of Magnesium Oxide Nanoparticles (MgO-NPs): A Promising Tool for Antimicrobial, Mosquitocidal Action, and Tanning Effluent Treatment. Journal of fungi (Basel, Switzerland), 7(5), 372**.**

Hagfeldt, A. and Grätzel, M. (2000): Molecular photovoltaics. Accounts of Chemical Research, 33(5): 269-277.

Immanuel, G.; Bhagavath, C.M.A.; Raj, P.I.; Esakkiraj, P. and Palavesam, A (2007): Production and partial purification of cellulase by *Aspergillus niger* and *A. fumigatus* fermented in coir waste and sawdust. The Internet Journal of Microbiology, 3(1): 1-20.

Jain, N.; Bhargava, A.; Tarafdar, J.C.; Singh, S.K. and Panwar, J. (2013): A biomimetic approach towards synthesis of zinc oxide nanoparticles. Applied Microbiology and biotechnology, 97(2): 859-869.

Kaul, R.K.; Kumar, P.; Burman, U.; Joshi, P.; Agrawal, A.; Raliya, R. and Tarafdar, J.C. (2012): Magnesium and iron nanoparticles production using microorganisms and various salts. Materials Science-Poland, 30(3): 254-258.

Kumar, R.; Liu, D. and Zhang, L. (2008): Advances in proteinous biomaterials. Journal of Biobased Materials and Bioenergy, 2(1): 1-24.

Latha, N. and Gowri,M. (2014): Biosynthesis and characterisation of Fe_3O_4 nanoparticles using *Caricaya papaya* leaves extract. International J Sci Res, 3: 1551–1556.

Lundblad, R.L. and Macdonald, F. (2010): Preparation of buffers for use in enzyme studies: G. Gomori. In Handbook of Biochemistry and Molecular Biology (pp. 739-742). CRC Press.

Mahdavi, V.; Prasad, T.N.V.K.V.; Reddy, A.V.B.; Reddy, B.R. and Madhavi, G. (2013): Application of phytogenic zerovalent iron nanoparticles in the adsorption of hexavalent chromium. Spectrochimica Acta PartA: Molecularand Biomolecular Spectroscopy, 116: 17-25.

Malik, L.A., Bashir, A., Qureashi, A. et al. (2019). Detection and removal of heavy metal ions: a review. Environ Chem Lett 17, 1495–152.

Mazumdar, H. and Haloi, N. (2017): A study on biosynthesis of Iron nanoparticles by *Pleurotus* sp. Journal of Microbiology and Biotechnology Research, 1(3): 39-49.

Moubasher, A.H. and Moustafa, A.F. (1970). A survey of Egyptian soil fungi with special reference to Aspergillus, Penicillium and Penicillium related genera. *Trans. Brit. Mycol. Soc.* 54: 35-44.

Muhiuddin G. et al. (2023) Synthesis of Ni doped barium hexa-ferrite by microemulsion route to enhance the visible light-driven photocatalytic degradation of crystal violet dye. 49(3): 4342-4355

Ninganagouda, S.; Rathod, V. and Singh, D. (2014): Characterization andbiosynthesis of silver nanoparticles using a fungus *Aspergillus niger*. International Letters of Natural Sciences, 10: 49-57.

Nithya, G.; Shepangam,N.H. and Balaji, S.(2011): Biosynthesis of silver nanoparticle and its antibacterial activity. Archives of Applied Science Research, 3(2): 377-380.

Petersen, N. O. (2017). Foundations for nano-science and nanotechnology. Engineering & Technology, Physical Sciences. 1st Edition. 360 pages. CRC Press.

Qayyum, S.; Khan, I.; Maqbool, F.; Zhao, Y.; Gu, Q. and Peng, C. (2016): Isolation and characterization of heavy metal resistant fungal isolates from industrial soil in China. Pak istan J. Zool. 48 (5): 1241-1247.

Rabie, G.H.; Hegazy, H.S.; Shaban, L.D. and Raie, D.S. (2015): Extracellular biosynthesis of bio-active nano-silver Using *Alfalfa* Seedling. Res. J. Pharm. Biol. Chem. Sci, 6: 87-93.

Raliya, R. (2013): Rapid, low-cost, and ecofriendly approach for iron nanoparticle synthesis using *Aspergillus oryzae* TFR9. Journal of Nanoparticles, V 2013, Article ID 141274, 4 pages.

Raliya, R. and Tarafdar, J.C. (2012): Novel approach for silver nanoparticle synthesis using *Aspergillus terreus* CZR-1: mechanism perspective. Journal of Bionanoscience, *6*(1): 12-16.

Raliya, R.; Tarafdar, J.C.; Choudhary, K.; Mal, P.; Raturi, A.; Gautam, R. and Singh, S.K.(2014a): Synthesis of MgO nanoparticles using *Aspergillus tubingensis* TFR- 3. Journal of Bionanoscience, 8(1): 34-38.

Raliya, R.; Tarafdar, J.C.; Singh, S.K.; Gautam, R.; Choudhary, K.; Maurino, V.G. and Saharan, V. (2014b): MgO nanoparticles biosynthesis and its effect on chlorophyll contents in the leaves of cluster bean (*Cyamopsis tetragonoloba L.*). Advanced Science, Engineering and Medicine, 6(5): 538-545.

Raper, K.B. and Fennell, D.I. (1965). The genus *Aspergillus*. *Williams and Wilkins Company, Baltimore, MD*.

Sarkar, J.; Mollick, M.M.R.; Chattopadhyay, D. and Acharya, K. (2017): An eco-friendly route of γ-Fe_2O_3 nanoparticles formation and investigation of the mechanical properties of the HPMC-γ-Fe_2O_3nanocomposites. Bioprocess and biosystems engineering, 40(3): 351-359.

Sastry, M.; Ahmad, A.; Khan, M.I. and Kumar, R. (2003): Biosynthesis of metal nanoparticles using fungi and actinomycete. Current science, 85(2): 162-170

Shafiq, S.A.; Al-Shammari, R.H. and Majeed, H.Z. (2016): Study of biosynthesis silver nanoparticles by *Fusarium graminaerum* and test their antimicrobial activity. International Journal of Innovation and Applied Studies, 15(1): p. 43.

Shah, S.; Dasgupta, S.; Chakraborty, M.; Vadakkekara, R. and Hajoori, M. (2014): Green synthesis of iron nanoparticles using plant extracts. Int J Biol Pharm Res, 5: 549–552

Subha Rajam, K.; Esther Rani, M.; Gunaseeli, R. and Hussain Munavar, M.(2013): Characterisation and antibacterial activity of silver nanoparticles synthesized by *Aspergillus* sp. Int J Pharm Bio Sci, 4(3): 748-57.

Sundaram, P.A.; Augustine, R. and Kannan, M. (2012): Extracellular biosynthesis of iron oxide nanoparticles by *Bacillus subtilis* strains isolated from rhizosphere soil. Biotechnology and bioprocess engineering, 17(4): 835-840.

Tarafdar, J.C.; Raliya, R. and Rathore, I. (2012): Microbial synthesis of phosphorous nanoparticle from tri-calcium phosphate using *Aspergillus tubingensis TFR-5. Journal of Bionanoscience, 6(2): 84-89.*

Tsivileva O, Pozdnyakov A, Ivanova AJM (2021). Polymer nano-composites of selenium biofabricated using fungi. 26(12): 3657 \ 57.

Vala, A.K.; Chudasama, B. and Patel, R.J. (2012): *Green synthesis of silver nanoparticles using marine-derived fungus Aspergillus niger. Micro & Nano Letters, 7(8): 859-862.*

Velu, M.; Lee, J.H.; Chang, W.S.; Lovanh, N.; Park, Y.J.; Jayanthi, P. and Oh, B.T. (2017): Fabrication, optimization, and characterization of noble silver nanoparticles from sugarcane leaf (Saccharum officinarum) extract for antifungal application. *3 Biotech, 7(2): p. 147.*

White, T.J. (1990). Amplification and direct sequencing of fungal ribosomal RNA genes for phylogenetics.

White, T. J., T. D. Bruns, S. B. Lee, and J. W. Taylor. Amplification and direct sequencing of fungal ribosomal RNA Genes for phylogenetics.

Woo, K.; Hong, J.; Choi, S.; Lee, H.W.; Ahn, J.P.; Kim, C.S. and Lee, S.W. (2004): Easy synthesis and magnetic properties of iron oxide nanoparticles. Chemistry of Materials, *16(14): 2814-2818.*

Yamini V, Rajeswari VDJJEN (2023). Effective bio-mediated nanoparticles for bioremediation of toxic metal ions from waste-water–A review. 12(2): 12–33.

Yaseen, T. and Yaseen, A. (2019*).* Wastewater treatment in removal of heavy metals: Nanotechnology applications in environmental engineering. In Nanotechnology Applications in Environmental Engineering (pp. 220-240).

Yong, P.; Rowson, N.A.; Farr, J.P.G.; Harris, I.R. and Macaskie, L.E. (2002): *Bioaccumulation of palladium by Desulfovibrio desulfuricans. Journal of Chemical Technology & Biotechnology, 77(5): 593-601.*

التخليق الفطري لجسيمات الهيماتيت (α-Fe_2O_3) النانوية باستخدام الفطريات وخواصها الفيزيائية والكيميائية وأنشطتها التحفيزية الضوئية.

حازم السيد كعبو[1]؛ محمود حسب الله سلطان[1]*؛ سعدالدين حسن[1]؛ هشام محمد مهدي[1]؛ إبراهيم سعيد[1]

[1] قسم النبات والميكروبيولوجي - كلية العلوم - جامعة الأزهر - مدينة نصر

* البريد الالكتروني للباحث الرئيسي : prof.mahmoud@Azhar.edu.eg

في هذه الدراسة تم تخليق الجسيمات النانوية بتقنية آمنه وفعالة لكونها صديقة للبيئة وقابلة للتطبيق على نطاق واسع. توضح الدراسة الحالية النهج الأخضر لتخليق جسيمات الهيماتيت النانوية باستخدام فطر *Aspergillus sydowii* ل FeSO4·7H2O كبادئ. عادة ما يكون التخليق الحيوي للهيماتيت مصحوبًا بتغير اللون من عديم اللون إلى اللون الأصفر كما يتم تقديرة باستخدام مقياس الطيف الضوئي للأشعة فوق البنفسجية.

يعتبر استخدام راشح الكتلة الحيوية لفطر *Aspergillus sydowii* في التخليق الحيوي لجسيمات الهيماتيت النانوية هو هدف العمل الحالي. تم دراسة الخواص التركيبية والبصرية للجسيمات النانوية الفطرية المنتجة باستخدام المجهر الإلكتروني النافذ (TEM)، ومطياف فورييه للأشعة تحت الحمراء (FTIR)، وحيود الأشعة السينية (XRD) وتشتت الضوء الديناميكي (DLS). وقد وجد أن جميع العوامل المدروسة وتفاعلاتها لها تأثير معنوي على الحجم البلوري، حسب النتائج. تراوح متوسط حجم قطر Fe_2O_3-NPs المُخلق حيويًا بين ٢٠ -٥٦ نانومتر. كان حجم Fe_2O_3-NPs المُخلق حيويًا ٢٨.٧ نانومتر، وتم تأكيد طبيعتها البلورية بواسطة XRD، وفقًا لنتائج التوصيف. تم الحصول على طيف رنين البلازمون السطحي من جسيمات الحديد النانوية عند ٣٧٠ نانومتر.تحت ضوء الأشعة فوق البنفسجية، تم تحلل أصباغ ريبازول الأسود ب والسفرانين والكريستال البنفسجي ضوئيًا باستخدام الجسيمات النانوية Fe_2O_3 المُخلقة حيويًا. أعلى نسبة إزالة اللون للريبازول الأسود ب والسفرانين والكريستال البنفسجي كانت ٩٢.١% ± ١.٢% و٧٠.١ ±٠.٨٨% و٩٤.٣% ± ٠.٩٣% على التوالي بعد ٩٠ و١٨٠ دقيقة، بالنسبة للريبازول الأسود ب والسفرانين والكريستال البنفسجي في الحضانة عند ٥٠.٠ ملجم/مل$^{-1}$ من Fe_2O_3-NPs. علاوة على ذلك، تم استخدام جزيئات الحديد النانوية بنجاح أكثر من مرة للتحلل الحيوي، وكان ذلك نظرا لفعاليته. تم استخدام جسيمات الهيماتيت النانوية لإزالة Cb وCo وPb وZn وCd، بنسب مئوية ٩٩.٧ ± ١.٢%، ٩٩.١% ± ١.٣%، ٩٧.١% ± ١.٣%، و٩٣.٨% ± ١.٤%، على التوالي. وأخيرًا، تم استخدام جسيمات الهيماتيت النانوية المُخلقة حيويًا في المعالجة الحيوية للمعادن الثقيلة ونشاط التحفيز الضوئي.

الكلمات المفتاحية: جسيمات النانو؛ الهيماتيت؛ التحفيز الضوئي؛ الفطريات؛ التخليق الحيوي؛ إزالة المعادن الثقيلة؛ الصبغات